International Communications in Heat and Mass Transfer 84 (2017) 110–120

Contents lists available at ScienceDirect

International Communications in Heat and Mass Transfer

journal homepage: www.elsevier.com/locate/ichmt

MHD effects and heat transfer analysis in magneto-thermo-fluid-structure coupled field in DCLL blanket

Long Chen, Mingjian Li, Mingjiu Ni, Nianmei Zhang*

School of Physics Science, University of Chinese Academy of Sciences, Beijing 100049, China

ARTICLE INFO

Keywords:
MHD effects
FCI
Magneto-thermo-fluid-structure coupled field
Thermal deformation

ABSTRACT

The study on DCLL blanket in ITER is related to magneto-thermo-fluid-structure coupled field issue. A key element in the DCLL concept is the flow channel insert (FCI) which serves as an electrical insulator to reduce the magnetohydrodynamic (MHD) pressure drop, and as a thermal insulator to decouple the high temperature PbLi from the reduced activation ferritic steel (RAFS) structure. In the present work, 16 geometrical models of flow ducts are introduced to study the MHD flow and heat transfer in DCLL blanket in magneto-thermo-fluid-structure coupled physical field. The PISO method on unstructured collocated meshes is applied to simulate the metal liquid flow and heat transfer in the blanket. The consistent and conservative scheme is employed to solve the incompressible Navier-Stokes equations with the Lorentz force included based on the electrical potential formula. The finite element method is used to study thermal mechanical behaviors of FCI. The velocity distribution, MHD pressure drop, electric current stream lines and temperature distribution in liquid blanket, thermal deformations of FCI in various geometrical models under external strong magnetic field are investigated. The pressure drop reduction factor is defined to analyze the influence of FCI structure on the MHD effects in the liquid metal blanket. The nonlinear coupling effects among magnetic field, heat transfer and FCI structure are revealed. The results show that thicker FCI and wider gap would increase the MHD pressure drops in bulk flow; the thicker FCI has smaller displacement but its strain and stress change non-monotonously; the wider gap can enhance the heat transfer performance but lead to larger stress in FCI. The optimal design is essential for the structural safety and high heat efficiency of the system.

1. Introduction

MHD effect and heat transfer are two key issues in the design of DCLL blanket [1–3]. The magnitude of the MHD pressure drops which are proportional to the electric current density induced in the fluid is determined by the resistance of the current patch. The MHD pressure drops increase with the increase of wall conductance ratio because of lower resistance compared to the insulating one. In order to reduce MHD pressure drop, flow channel insert (FCI) made of SiC_f/SiC which has relatively low electrical conductivity, is introduced to decouple the liquid metal from the walls and to reduce the electric current. Another main attraction of the FCI is related to low thermal conductivity of the SiC_f/SiC, allowing for the reduction of heat losses from the breeder and both increasing high bulk temperatures at the blanket exit and decreasing the temperature of first wall in order to meet the design limit [4].

In the past, several overviews of liquid metal MHD flows in fusion relevant condition have been carried out, focusing on the blanket issues common to all types of liquid metal blankets, such as velocity and temperature field distribution, the MHD pressure drop, complex geometries flows and heat transfer [5–8]. Velocity profiles of MHD flow in the front poloidal channel of the DCLL blanket were studied by Smolentsev et al. [9] based on a 2D model for a fully developed flow. However, it has been verified [10,11] that the liquid metal fluid in rectangular duct relevant to fusion blanket using FCI made of conductive or insulated walls with/without slot is a fully 3D flow. Pressure gradient in the flow direction can be divided into two stages, including changing pressure gradient of developing length around 4–5 times of the half channel width and constant pressure gradient. The detailed MHD and thermal issues of the SiC_f/SiC FCI analysis for Pb—Li flows are also presented in [12] by Smolentsev. In this paper, two FCI modifications, one with no pressure equalization openings and one with a pressure equalization slot, have been considered. They focused on studying the effects of electric and thermal conductivity of the SiC_f/SiC on the MHD pressure drop and reduction of heat leakage from the breeder into the helium flows. The role of the pressure equalization

* Corresponding author.
E-mail address: nmzhang@ucas.ac.cn (N. Zhang).

http://dx.doi.org/10.1016/j.icheatmasstransfer.2017.04.009

Available online 12 April 2017

openings have been discussed, too. In 2008, Smolentsev et al. [13] summarized the important blanket feasibility issues, such as the MHD pressure drop, heat leakages from PbLi into the cooling helium flows, and the temperature distributions in the insulating flow insert and at the material interface. They pointed out high interface temperature between PbLi and the ferritic wall may exceed the allowable material limits. Recently, Sutevski et al. [14] have studied two pressure equalization (PE) mechanisms. The paper suggested that PE via electric currents appears to dominate compared to purely hydrodynamic PE. They addressed the impact of the FCI electrical conductivity, slot size, and the duct length and recommended that a PES does not contribute significantly to PE. However, research on the effects of FCI thickness or gap width on the MHD and thermal issues, including MHD pressure drop, heat transfer, thermal stresses and thermal deformation, has not been achieved so far. After numerous 3D simulations, we find that the influences of geometrical characteristics are nonlinear and the coupling effects of FCI thickness and gap width play a key role on structural safety and heat transfer efficiency.

In fact, the DCLL blanket endures affection from both external strong magnetic field and large gradient neutron flux. The metal fluid, FCI structure, magnetic field and heat source constitute a coupling physical field. The high neutron flux formula from neutron analysis [15] demonstrates the relation between space location and heat magnitude. It implies that geometrical configuration of blanket would cause the variation of not only metal liquid flow but also heat amount from neutron reaction. The flow velocity field, temperature distribution and thermal mechanical behaviors of FCI would change accordingly. In this work, MHD of metal fluid, heat transfer and thermal deformation of FCI are investigated applying 3D CFD simulating code and FE (finite element) code.

The paper is organized as follows: Section 2 describes the general MHD problems in liquid metal blanket applications, including geometry and material properties. Section 3 introduces the mathematical formula applied in this simulation, including governing equations in fluid field and solid field, boundary conditions on fluid-structure interfaces and the numerical method. The algorithm employed is stated and code developed on the basis of FVM is validated in Section 4. Section 5 addresses the results and analyzes the particular MHD issues, including MHD pressure drop, heat transfer phenomena, distribution of temperature field, heat leakage into He, and thermal stresses and deformation. Section 6 summarizes the conclusion by analysis of the simulation.

2. Description for physical model

The configuration of simplified DCLL blanket channel model with a FCI is illustrated in Fig. 1. In the cross-section view, the outer steel duct is cooled by helium. Laminar flows of liquid metal through a straight rectangular duct under a transversal strong magnetic field are considered. The FCI is separated from the ferritic wall by a thin gap filled with liquid metal. These gaps can avoid strong mechanical interaction between the FCI and the ferritic wall with lower temperature. In the following parts, flow inside the FCI is called “bulk flow”, and flow between FCI and ferritic wall is called “gap flow”.

In our simulation, liquid metal flows along the poloidal direction (z-direction) with the length of the channel from z = 0 to 2000 mm. The current simulation is performed with a uniform strong magnetic field B_0 = 1 T paralleling to toroidal direction (y-direction), as shown in Fig. 1. The inlet velocity u_0 is 0.06 m/s and inlet temperature is 733 K for bulk flow and gap flow. The radial direction is set to be along x-direction, as shown in Fig. 1. The physical parameters of the liquid metal, FCI and ferritic wall are provided in Table 1.

As previously mentioned, FCI thicknesses and gap widths could affect flow patterns under strong magnetic field, temperature distributions and structural stresses of FCI in the blanket module. On the other hand, the pressure and temperature of fluid directly influence the deformations and stresses of FCI structure. Therefore, study on the interactions of metal fluid and FCI structure plays dominant role in blanket design. In order to investigate such influences caused by geometrical characteristics, a series of models are carried out for analysis of flow and heat transfer and structural optimization. In the present work, we focus mainly on analyzing the effects of the FCI thickness and gap widths on the MHD pressure drops and heat transfer. Cases with 16 geometrical models are listed in Table 2. For the 16 designs, the volume of the simulation region $224\ mm \times 324\ mm \times 2000\ mm$ is kept constant. Here, FCI thicknesses are considered as 2 mm, 3 mm, 5 mm and 7 mm while gap widths are 2 mm, 4 mm, 6 mm and 8 mm. The regions of bulk flow are adjusted according to the thickness of FCI and width of gap.

3. Mathematical formulation for magneto-thermo-fluid-structure coupled field

For the magneto-thermo-fluid-structure multi-physical field, the effect of strong magnetic field is reflected in pressure and shear stress of fluid by Lorentz force. The heat source produced by neutron reaction impacts the deformations and stresses of the structure by bulk flow. So, the fluid field and solid field can be considered to be two main parts of the coupling field. The external magnetic field, metal fluid and neutronic heat flux coexist in fluid field. The solid field includes FCI structure and temperature field. Herein, the sequential method is used to simulate fluid flow, temperature distribution and thermal deformation of FCI and investigate the fluid-structure interaction.

3.1. Governing equations for MHD flow

The flow of viscous incompressible electrically conducting fluid under a uniform external magnetic field can be described by the Navier-Stokes Eqs. (1) and (2), representing the conservations of momentum and mass. And electrodynamics Eqs. (3) and (4) state the Ohm's law and charge conservation [16]. The two sets of equations are coupled by Lorentz force ($\boldsymbol{J} \times \boldsymbol{B}$) and induced electric current field $\boldsymbol{u} \times \boldsymbol{B}$. The energy equation is described by formula (5).

$$\frac{\partial \boldsymbol{u}}{\partial t} + \boldsymbol{u}\cdot\nabla\boldsymbol{u} = -\frac{1}{\rho}\nabla p + \nabla(\nu\nabla\boldsymbol{u}) + \frac{1}{\rho}(\boldsymbol{J}\times\boldsymbol{B}) \tag{1}$$

$$\nabla\cdot\boldsymbol{u} = 0 \tag{2}$$

$$\boldsymbol{J} = \sigma(-\nabla\varphi + \boldsymbol{u}\times\boldsymbol{B}) \tag{3}$$

$$\nabla\cdot\boldsymbol{J} = 0 \tag{4}$$

$$\rho C_p\left(\frac{\partial T}{\partial t} + \boldsymbol{u}\cdot\nabla T\right) = \nabla\cdot(K\nabla T) + \frac{\boldsymbol{J}^2}{\sigma} + Q \tag{5}$$

Here $\boldsymbol{u}$, p, $\boldsymbol{J}$, φ, T are the main variables according to velocity vector, kinetic pressure, electric current density, electrical potential and temperature, respectively. $\boldsymbol{B}$ stands for the magnitude of external magnetic field. Fluid properties are ν, σ, K, C_p, ρ, corresponding to the fluid viscosity, electric conductivity, thermal conductivity, specific heat capacity and fluid density. Q is the thermal load deposited by the high neutron flux, $Q = 3\times10^7 e^{-10(x+b)}$, where b is the half length of bulk flow along the X direction.

In this work, a dimensionless parameter, Hartmann number $Ha = aB\sqrt{\sigma/\rho\nu}$, is employed to express the balance of forces established between the electromagnetic force and the viscous force.

3.2. Governing equations for solid structure

Geometric equation for small deformation in FCI considering temperature effect is

$$\varepsilon_{ij} = \frac{1}{2}(d_{i,j} + d_{j,i}) + \alpha\Delta T\delta_{ij} \tag{6}$$

where, ε_{ij} represents strain tensor, and d_i represents displacement

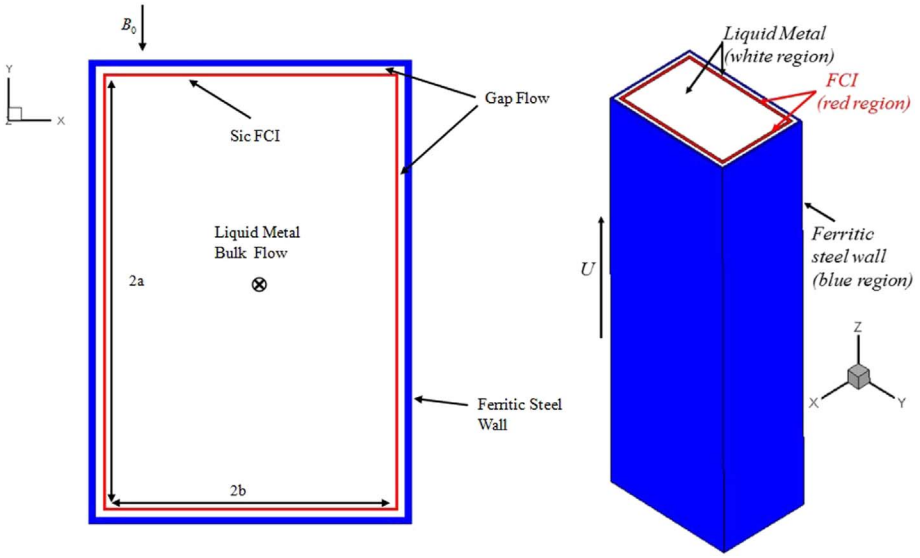

Fig. 1. Configuration of poloidal duct with silicon carbide (SiC) flow channel insert (FCI).

vector, and ΔT describes the temperature variation of solid structure and α is thermal expansion coefficient. δ_{ij} is the Kronecker delta.

$$\left.\begin{aligned}\delta_{ij} = 1 (i = j)\\ \delta_{ij} = 0 (i \neq j)\end{aligned}\right\} \tag{7}$$

FCI is made of SiC material. As described by Abdou et al. [17], SiC is the candidate material for FCI because of its good electrical and heat insulating characteristic. And its constitutive relation meet generalized Hooke law in elastic state. Considering the small deformation of FCI structure, the constitutive equation would describe the linear relation between strains and stresses.

$$\sigma_{ij} = 2G\varepsilon_{ij} + \lambda\Theta\delta_{ij} \tag{8}$$

Here, σ_{ij} is defined as stress tensor. G is shear modulus and $\lambda = E\mu/[(1+\mu)(1-2\mu)]$ is Lame constant. $\Theta = \varepsilon_{ii}$ is volumetric strain and μ is Poisson ratio.

And the equilibrium equations of structure satisfy

$$\sigma_{ij,j} + F_i = 0 \tag{9}$$

where, F_i is the ith component of volumetric force.

3.3. Boundary condition

A uniform velocity and temperature are specified as inlet boundary condition, and the pressure at outlet is set to be zero. On the gap flow-outer wall of FCI structure interface and bulk flow-inner wall of FCI structure interface, solutions are coupled by ensuring the continuity of wall temperature, wall electric potential and wall normal current.

$$T_f = T_w \tag{10}$$

$$q_w'' = q_f'' \tag{11}$$

$$\varphi_f = \varphi_w \tag{12}$$

Table 2
Geometrical parameters (millimeter) for the front poloidal channel of the reference DCLL blanket.

FW	5	5	5	5	5	5	5	5	5	5	5	5	5	5	5	5
Gap	2	4	6	8	2	4	6	8	2	4	6	8	2	4	6	8
FCI	2	2	2	2	3	3	3	3	5	5	5	5	7	7	7	7

$$j_{n,f} = j_{n,w} \tag{13}$$

Here, T_f and T_w express temperature of fluid and structure wall. φ_f and φ_w express electric potentials of fluid and structure wall. $j_{n,f}$ and $j_{n,w}$ express normal currents of fluid and structure wall. q_w'' and q_f'' describe heat fluxes on solid section and fluid section of fluid-solid interface, respectively.

Simultaneously, non-slip boundary conditions are applied for velocity and Neumann conditions are set up for pressure on fluid-structure interfaces.

The thermal condition of FCI and FW at z = 0 and z = 2000 mm is set to be insulation $\frac{\partial T}{\partial n} = 0$, while the outside walls of the FW are set to satisfy convective boundary condition.

$$K\frac{\partial T}{\partial n} + h(T - T_{ref}) = 0 \tag{14}$$

Here, h is convective heat transfer coefficient. The temperature in the helium flows T_{ref} is fixed to be 400°C, and the heat transfer coefficient in the helium flow is 4000W/m^2·K.

Because the normal component of current density is zero, Neumann condition of electrical potential is specified for the insulated walls

$$\frac{\partial \varphi}{\partial n} = 0 \tag{15}$$

Table 1
Physical parameters of the materials.

	Density (kg/m^3)	Dynamic viscosity (kg/(m·s))	Electrical conductivity (S/m)	Specific heat capacity (J/(kg·K))	Thermal conductivity (W/(m·K))	Elastic modulus (GPa)	Poisson's ratio	Thermal expansion coefficient (K^{-1})
Liquid metal	9500	0.001786	850,000	190	16			
FCI	2500		0.0001	1200	8	2E2	0.2	3.3E-06
FW	7850		1,230,000	480	30			

4. Numerical algorithm and code validation

4.1. Algorithm for metal fluid flow

In the build-up of the present numerical code, PISO [18] algorithm is introduced to treat the pressure-velocity coupling equations including the Lorentz force term in fluid field. The finite volume method is employed to discrete the incompressible Navier-Stokes equations, electrodynamics equations and energy equation in the node-based formulation. 3D simulating code is developed on the basis of OpenFOAM. The PISO loop consists of an implicit momentum predictor followed by a series of pressure solutions and explicit velocity corrections. The loop is repeated until a pre-determined tolerance is reached. During the loop, the Lorentz force term is treated explicitly as an additional force term.

In simulation of MHD effect, the calculation of Lorentz force at moderate and high Hartmann numbers is a very challenging part. In the work, the electric Poisson equation is solved according to the consistent and conservative scheme [19–21] by satisfying boundary conditions (12) and (13).

In order to guarantee the continuity of temperature and heat flux at the interface, boundary conditions (10) and (11) are introduced to calculate the temperature distribution in FW-gap flow-FCI-bulk flow coupled physics field.

4.2. Grids for coupled field

Because of external magnetic field, the metal fluid flow is impacted by induced Lorentz force. The sharp velocity gradient occurs near side wall which is paralleled to the magnetic field. Therefore, for the present work, the grid spacing is decreased greatly closer to the wall to ensure that the great gradient can be captured accurately, as shown in Fig. 2.

4.3. Simulation for structural deformations and stresses

For solid field, finite element method was used to solve deformation, stress and strain in FCI. In order to improve the accuracy of computation, 20 node hexahedral elements are applied to investigate the mechanical behaviors of FCI under coupled field of temperature and fluid flow. In this process, both thermal effect and pressure impact from fluid are considered. On the fluid-structure interfaces between either gap flow and FCI or bulk flow and FCI, the following boundary conditions are satisfied.

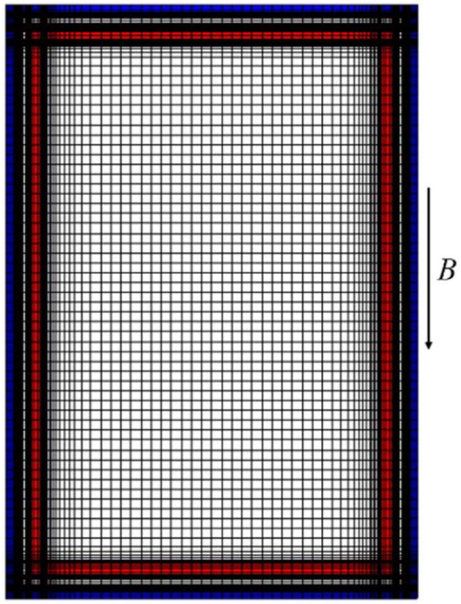

Fig. 2. Meshes in gap flow-FCI-bulk flow coupled field.

$$T_f = T_w,\ p_f = p_w \tag{16}$$

4.4. Validation

To validate the code developed for the solution for MHD flows, two benchmark problems are simulated. A solution of MHD flow in pipe channel is employed to check the accuracy of the developed code with non-orthogonal meshes. The simulation results match the reference solutions [22] very well, as seen in Fig. 3.

The second problem is Hunt's analytical solution of MHD flow in ducts [23]. The goal is to check the ability of the code for MHD flow with high Hartmann number. The velocity profiles of $Ha = 20{,}000$ shown in Fig. 4 is in good agreement with Hunt's solution.

To validate the finite element solver applied in the solid region, a thermal stress case of tube is conducted. In this case, a thick wall tube with inner radius r_a and outer radius r_b is considered. The temperature difference between its inner surface and outer surface is T_a, and the tube has thermal insulated and traction-free ends. The material of the tube has elastic modulus E, Poisson's ratio μ and linear thermal expansion coefficient α. The radial, toroidal and poloidal directions are described by subscripts r, ϕ and z, respectively. According to classic elasticity theory [24], the radial, toroidal and poloidal thermal stresses along the radial direction can be denoted as follows.

$$\sigma_r = -\frac{E\alpha T_a}{2(1-\mu)}\left[\frac{\ln\frac{r_b}{r}}{\ln\frac{r_b}{r_a}} - \frac{\frac{r_b^2}{r^2}-1}{\frac{r_b^2}{r_a^2}-1}\right] \tag{17}$$

$$\sigma_\varphi = -\frac{E\alpha T_a}{2(1-\mu)}\left[\frac{\ln\frac{r_b}{r}-1}{\ln\frac{r_b}{r_a}} + \frac{\frac{r_b^2}{r^2}+1}{\frac{r_b^2}{r_a^2}-1}\right] \tag{18}$$

$$\sigma_z = -\frac{E\alpha T_a}{2(1-\mu)}\left[\frac{2\ln\frac{r_b}{r}-1}{\ln\frac{r_b}{r_a}} + \frac{2}{\frac{r_b^2}{r_a^2}-1}\right] \tag{19}$$

In this work, a case with steel tube under 60 K temperature difference between inner and outer surface is presented for validation. With appropriate grids, good accuracy can be obtained here. As can be seen in Fig. 5, numerical results of radial, toroidal and poloidal thermal stresses all have good agreements with analytical results. And the average numerical error in this case is within 0.5% compared with analytical solutions.

5. Simulation results and analysis

5.1. Basic MHD effects

When insulated FCI is introduced into the blanket, the stream line of current is cut off due to the low electrical conductivity of FCI. The FCIs decouple electrically the PbLi flow from the steel walls by interrupting the current paths towards the conducting walls. In the insulated ducts, the flows fully match the Shercliff flow. There are four current loops which is asymmetry because of different conductivities of FCI and wall located in the lower and upper sections of the gap. As shown in the Fig. 6(b), velocity inside insulated FCI is almost uniform which is much smaller than that outside FCI. In the Hartmann gaps, the flow is almost stagnant. However, in each side gap, it can be found that a lower velocity jet located at the electrically conducting wall and a higher velocity jet located at the non-conducting wall.

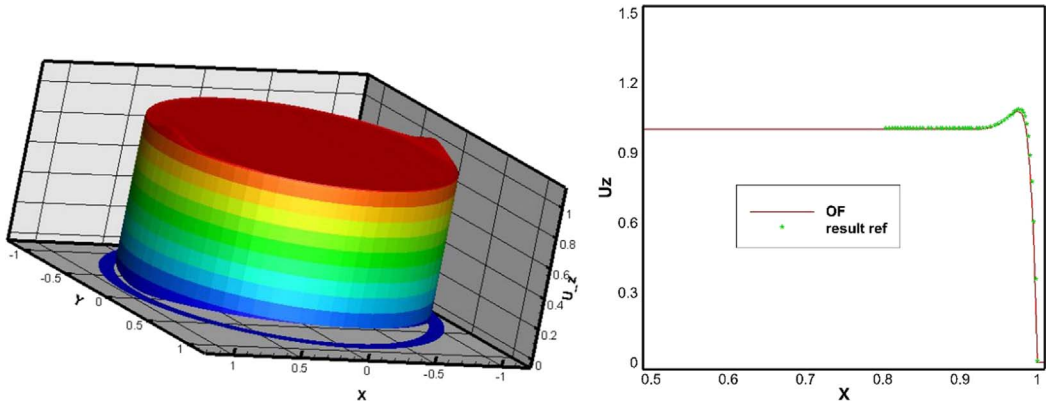

(a)Velocity contours in 3D (b) velocity profile along the line y=0

Fig. 3. MHD flow in a perfect conducting pipe, at $Ha = 2000$.

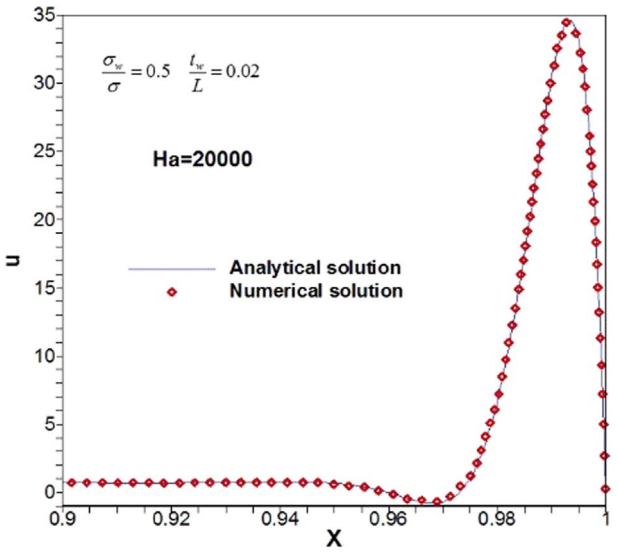

Fig. 4. Comparison of velocity profiles with the Hunt's case.

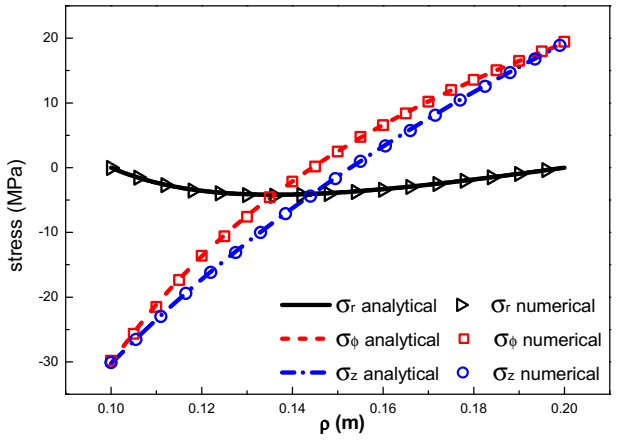

Fig. 5. Validation case for thermal stress calculation.

5.2. MHD pressure drop

MHD pressure variation along the poloidal direction is shown in Fig. 7. In order to investigate the effects of FCI on pressure drop reduction, we also calculated a case without FCI for comparison. It can be seen clearly, an insulated FCI can greatly decrease pressure difference, comparing with the no-FCI case. FCI would have strong impact on the pressure in bulk flow, Hartmann gap flow and side gap flow. The reason is that electric insulated FCI change the electric potential and electric current distribution. The Lorentz force changed would break the equilibrium of force in fluid field. Correspondingly, pressure distribution of fluid is changed.

A MHD pressure drop reduction factor R is defined to describe the effect of pressure drop reduction compared to case with FCI.

$$R = \frac{(dp/dz)_{No-FCI}}{(dp/dz)_{FCI}}$$

Where, $(dp/dz)_{FCI}$ represents the MHD pressure drop of bulk flow with FCI and $(dp/dz)_{NO-FCI}$ represents the MHD pressure drop for the case without FCI. Fig. 8 shows that the MHD pressure drop reduction factor reaches the highest value, 116.2, when the FCI thickness is 2 mm and the gap width is 2 mm. In contrary, the reduction factor reaches the lowest value 108.2 when the FCI thickness is 7 mm and the gap width is 8 mm. It is clear that there exist small differences among the pressure drop factors for 16 blanket models. But any one of 16 models can reduce the pressure drop over 100 times.

Fig. 9 shows the comparison of MHD pressure drop in bulk flow and Hartmann gap flow for different FCI thickness and gap width. The pressure drop Δp means the max difference between inlet pressure and outlet pressure. As illustrated in Fig. 9(a), thicker FCI and wider gap will lead to larger pressure drop in bulk flow. For the same gap width, as the increase of FCI thickness, the size of the bulk region shrinks. Accordingly, smaller metal fluid flow region reduces the current loops and the current density and Lorentz force increase as a result. It is the same reason for the case of increasing gap width. Fig. 9(b) shows that wider gap would reduce pressure drop in gap flow while FCI thickness affect little to gap flow pressure drop with the same gap width. Compared with pressure drop in gap flow, pressure drop of bulk flow can be neglected. Consequently, in order to reduce pressure drop and pumping power in the blanket module, we have better to choose a wider gap.

5.3. Effects of geometry configuration on the heat transfer

In order to study the effects of FCI thickness on the heat transfer, 16 configurations mentioned above are conducted. Temperature field in bulk flow, gap flow, FCI and ferritic steel wall will be analyzed. The key points in the heat transfer optimizations are focused on improvement of exit temperature of liquid metal, minimization of heat losses from the liquid metal, lower fluid-solid interface temperature which should be below corrosion limit of solid material and reduction of temperature stresses in the FCI.

The typical temperature distributions at the outlet and in the poloidal-radial plane of the flow channel are illustrated in Fig. 10(a)

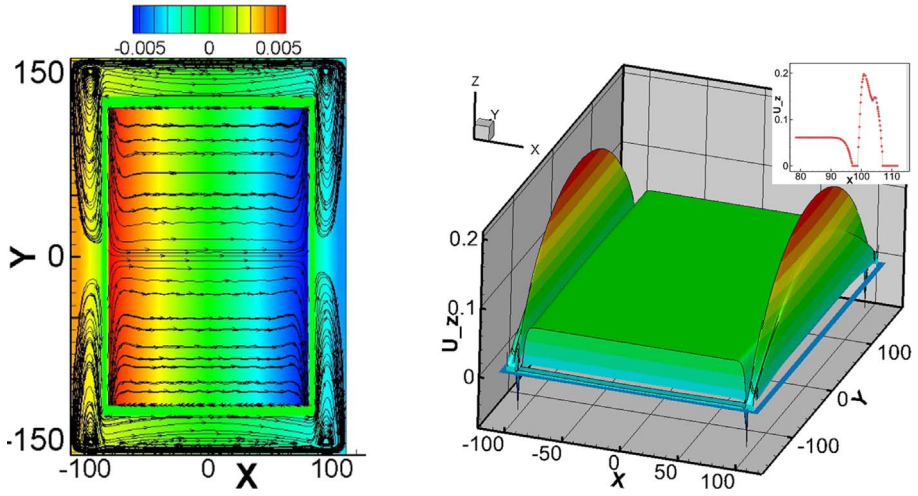

(a) Electric potential and current streamlines (b) velocity field

Fig. 6. The distribution of velocity field, electric potential and current streamlines at outlet (FCI 2 mm, gap 8 mm).

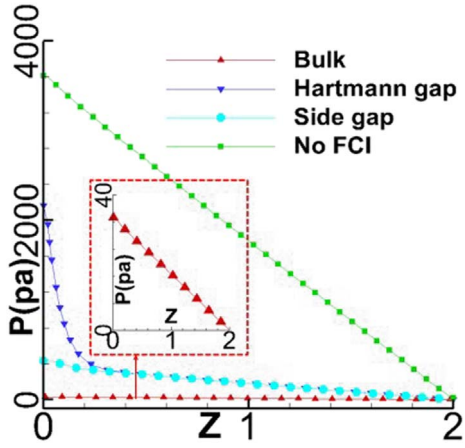

Fig. 7. Pressure filed along the flow direction (FCI 2 mm, gap 5 mm).

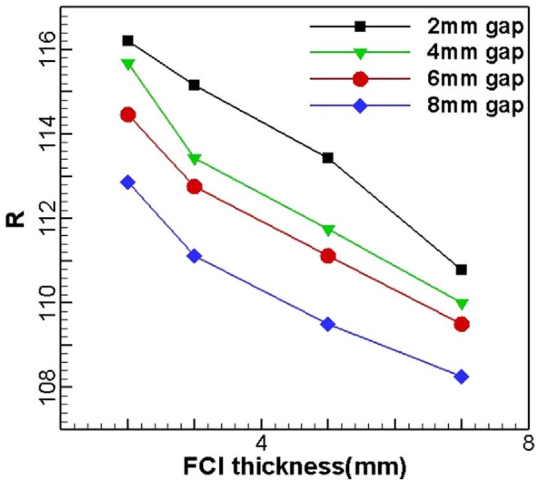

Fig. 8. Effect of the blanket configuration on the MHD pressure drop reduction factor R in bulk flow.

and (b), respectively. As can be seen, in the bulk flow, temperature field varies intensely in the radial (X) direction while changes gently in the toroidal (Y) direction. However, in both radial and toroidal direction, the changes in temperature field are large near the inside ferritic steel wall cooled by the helium flows. Because of the heat transfer by the liquid metal, temperature filed achieves the peak value at the exit.

To analyze the effects of FCI thickness on improvement of temperature of liquid metal, temperature distribution in the vicinity of first wall (FW) at the exit and the temperature on first wall inside surface are drawn in Fig. 11(a) and (b). Increasing the FCI thickness, the bulk flow carries more heat and exit temperature increases. Heat leakage from bulk flow into gap flow and steel wall is reduced and gap flow temperature and temperature on the first wall surface decrease, consequently. The max temperature at the exit is affected obviously by FCI thickness and increases as the FCI thickness increases, because thicker FCI becomes a better thermal insulator. To the same energy poured into the system, the exit temperature becomes higher. Meanwhile, the increasing of FCI thickness results in a lower max interface temperature. This is because that the function of FCI for preventing the high energy transfer transversely from bulk flow to Fe wall becomes stronger as the thickness of FCI increases.

The velocity fields near FW drawn in Fig. 12(a) imply that wider gap would lead to higher jet velocity in side gap flow, which enhance the heat transfer performance. The reason is that gap flows with higher velocity would carry more heat away from the duct. Meanwhile, the convective heat transfer performance between helium and steel wall would be better and plays an important role to the temperature of the first wall. The gap flow temperature and the bulk flow temperature near the hotter side wall of FCI are reduced. The temperature variations are shown in Fig. 12(b).

Changes of the exit temperature due to various gap widths are small. When gap is wider, the cross-sectional area and flow rate in gap will be larger, and heat transfer can be enhanced, thus temperature on first wall will be lower, as illustrated in Fig. 13. Overall, wider gap is still preferred because of the lower interface temperature.

The peak temperature at the interface between Fe and gap flow for all the 16 cases are shown at Fig. 14. The increasing of FCI thickness prevents the high energy transfer transversely from bulk flow to Fe wall which reduces the heat transfer efficiency. With the increasing of the gap width, the velocity of jet flow in side gap increases which enhances the effects of heat transfer and decreases the temperature at the interface between Fe wall and gap flow. The interface temperature reaches the highest value 530°C, when the FCI thickness is 2 mm and the gap width is 2 mm. Otherwise, when the FCI thickness is 7 mm and the gap width is 8 mm, the interface temperature reaches the lowest value 460°C. The data shows that thicker FCI and wider gap is beneficial for the FW safety.

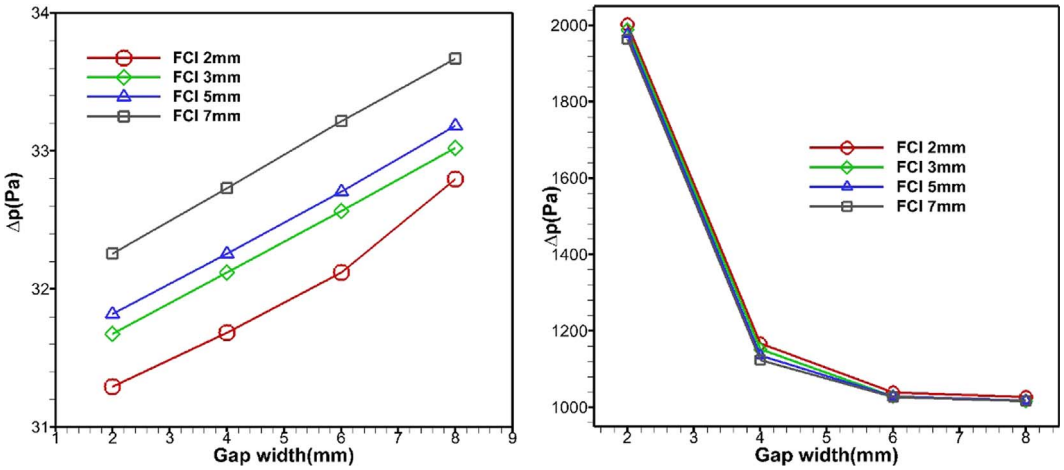

Fig. 9. Effect of the FCI thickness and gap width on the MHD pressure drop.

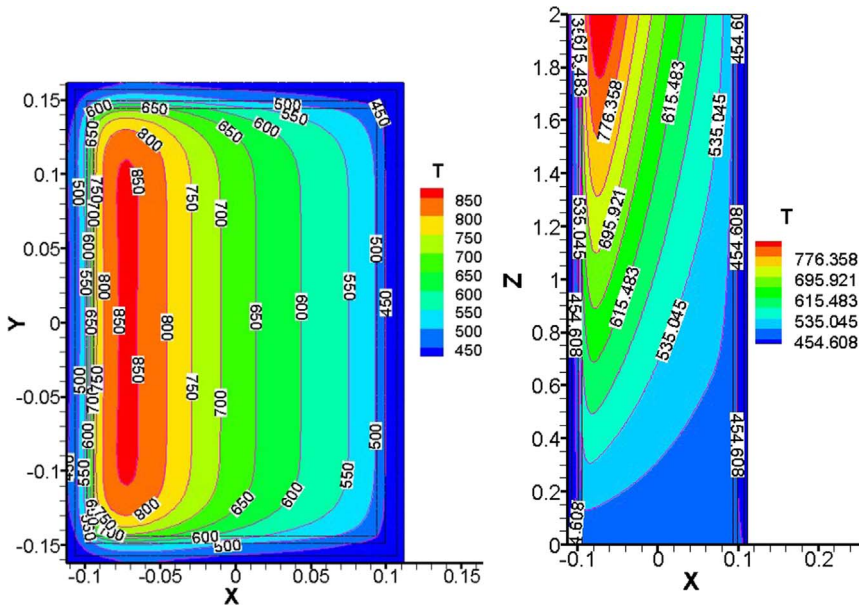

Fig. 10. Temperature field in the blanket channel.

5.4. *Effects of the FCI thickness and gap width on mechanical behaviors of FCI*

Fig. 15 illustrates that the radial displacements would not change obviously with increasing gap width. Because the temperature difference through FCI thickness depends on both the heat amount carried away by poloidal flow of metal fluid in bulk and gap and heat transfer with the FW cooled by Helium coolant. Although the velocity of gap flow is higher and the MHD effect is enhanced when the gap width changes from 2 mm to 8 mm, the temperature differences through the hotter side wall have very small variations. Therefore, there exist some slight radial displacement changes (can be seen in Fig. 15(a) and (c)) on hotter side wall of FCI when gap width is increased. Meanwhile, wider gap can only increase the toroidal displacement of Hartmann wall slightly as shown in Fig. 15(b) and (d).

The Mises stresses of side wall and Hartmann wall are displayed in Fig. 16. When gap is thinner, the velocity of gap flow is lower. The strain and stress of FCI are bigger because of the slightly increasing of temperature difference through the FCI thickness.

The radial displacements on hotter side wall and toroidal displacements on Hartmann wall are demonstrated in Fig. 17(a) and (b), while Fig. 17(c) and (d) are the contours of displacement vector sum. The displacements of structure mainly depend on two factors: structural stiffness and temperature difference through the wall thickness. When increasing the FCI thickness, the temperature differences through the FCI hotter side wall change very small. The stiffness of FCI plays dominant role in the displacements. Hence, the thicker FCI would have smaller radial displacements in hotter wall because of its better stiffness, as illustrated in Fig. 17(a). While in Fig. 17(b), temperature factor dominates the stiffness factor and lead to larger toroidal displacement in thicker FCIs. Comparing with the Fig. 15, it can be found easily that the FCI thickness has stronger influence on the heat transfer and mechanical behaviors of FCI than the gap width does. The maximum radial displacements of hotter side wall are about 10 times of the maximum toroidal displacements of Hartmann wall. And from Fig. 17(c) and (d), we can see that radial and poloidal displacements

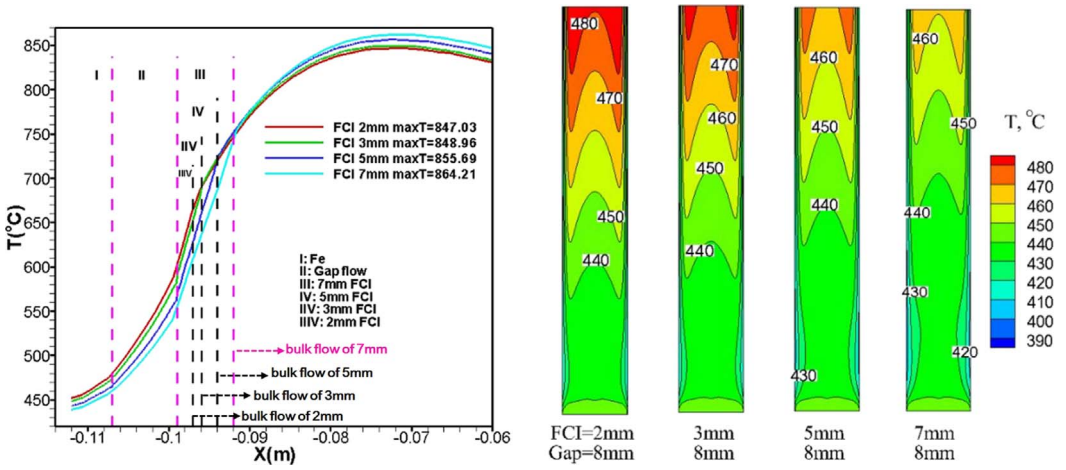

(a)Temperature distributions at Y=0, Z=2 (b) Temperature on FW inside surface with gap width 8mm and FCI thickness 2mm, 3mm, 5mm, 7mm

Fig. 11. Temperature distribution v.s. FCI thickness.

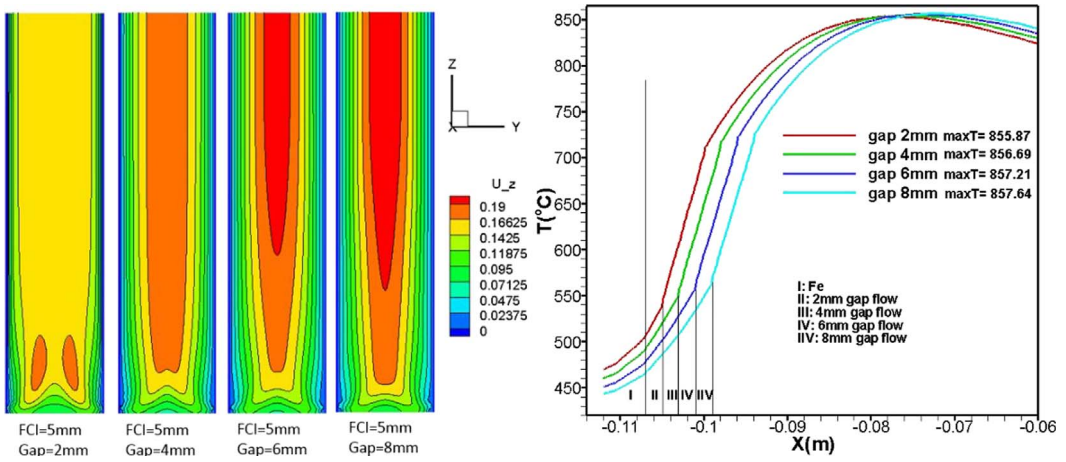

(a) Velocity contours near FW (b) Temperature distributions at Y=0, Z=2

Fig. 12. Velocity and temperature distribution with FCI thickness 5 mm and gap width 2 mm, 4 mm, 6 mm, 8 mm.

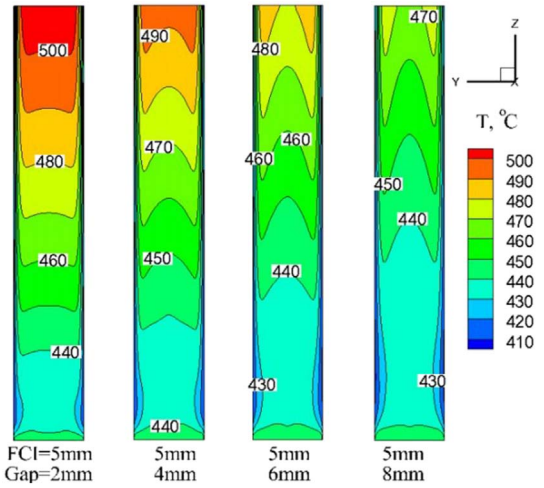

Fig. 13. Temperature on FW inside surface.

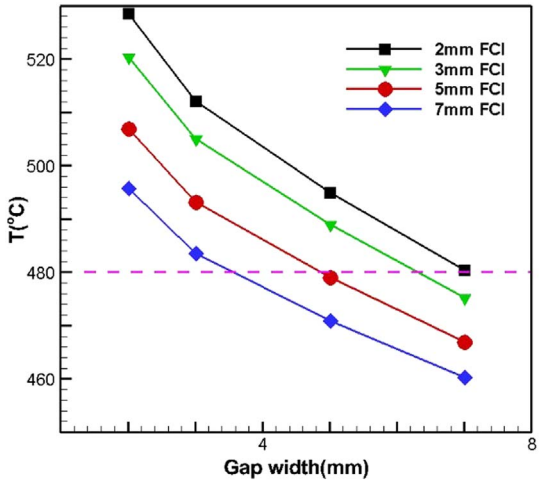

Fig. 14. Peak temperature of Fe wall v.s. gap width.

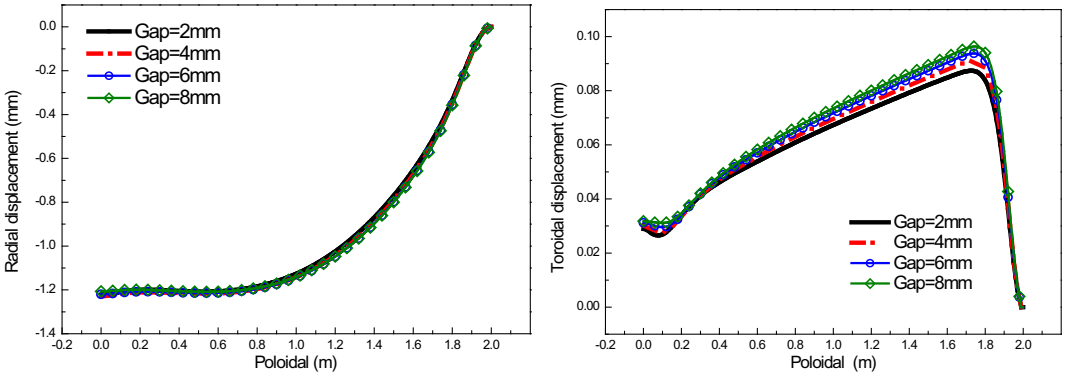

(a)Maximum Radial displacements on hotter side wall

(b) Toroidal displacements at X=0 on Hartmann wall

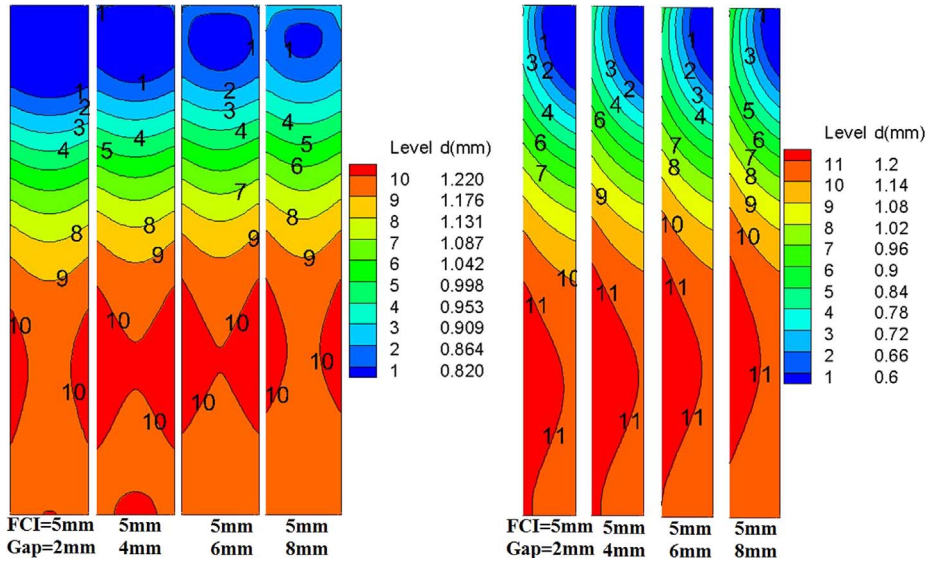

(c) Radial displacement contours on hotter side wall

(d) Toroidal displacement contours on Hartmann wall

Fig.15. FCI displacements at side wall and Hartmann wall

Fig. 15. FCI displacements at side wall and Hartmann wall with gap width 2 mm, 4 mm, 6 mm and 8 mm.

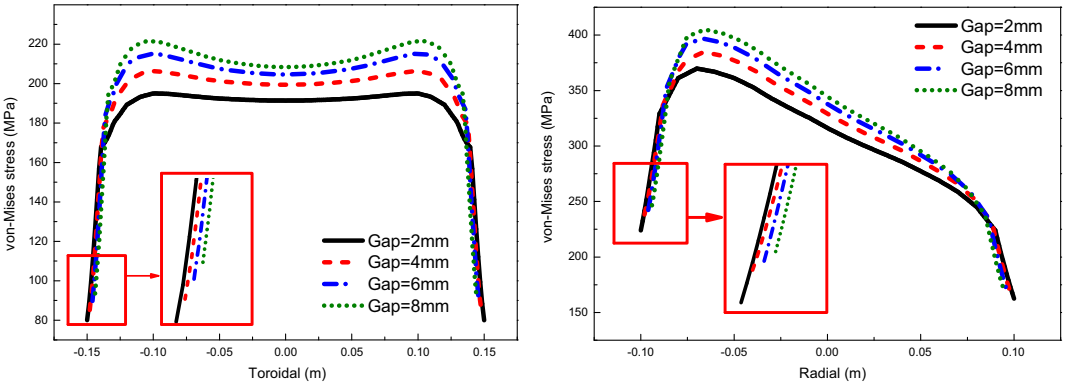

(a) von-Mises stresses on side wall

(b) von-Misesstresses on Hartmann wall

Fig. 16. Von-Mises stresses at side wall and Hartmann wall of FCI with gap width 2 mm, 4 mm, 6 mm and 8 mm.

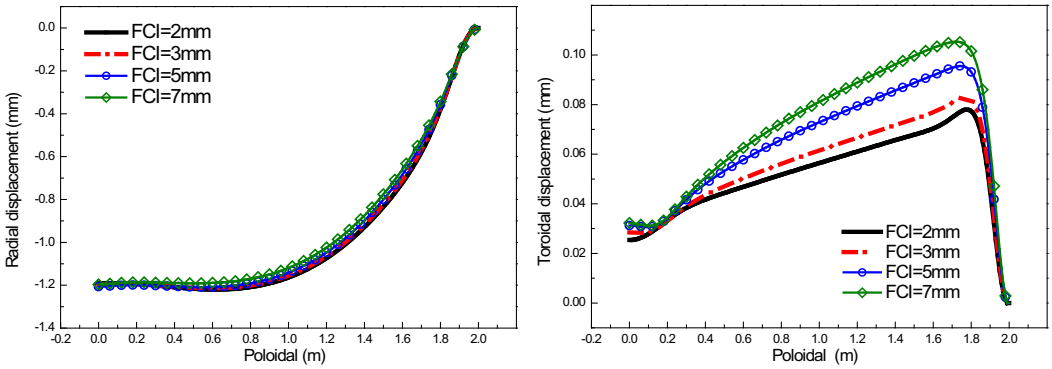

(a) Maximum Radial displacements on hotter side wall (b) Toroidal displacement at X=0 on Hartmann wall

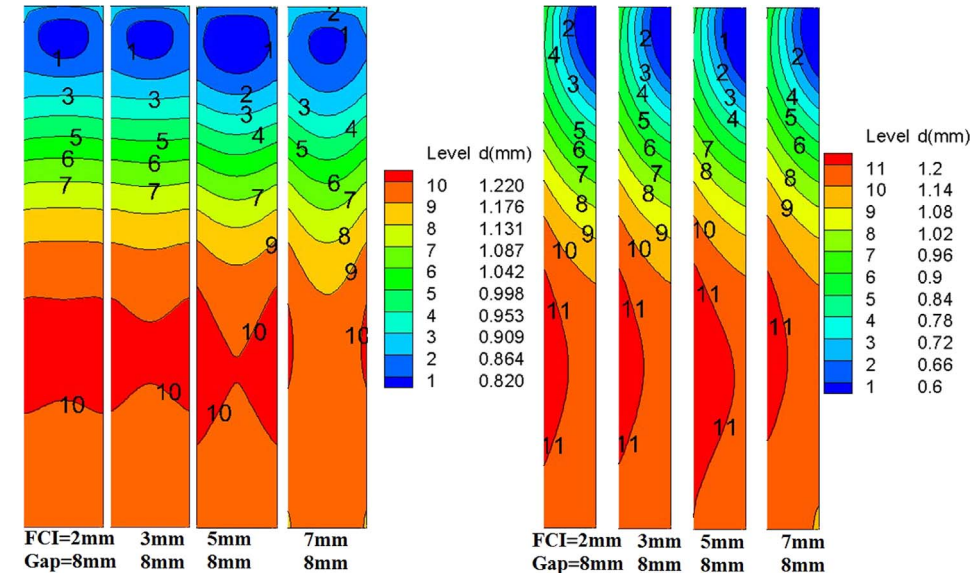

(c) Radial displacements on hotter side wall (d) Toroidal displacements at X=0 on Hartmann wall

Fig. 17. Displacements at side wall and Hartmann wall with FCI thickness 2 mm, 3 mm, 5 mm and 7 mm.

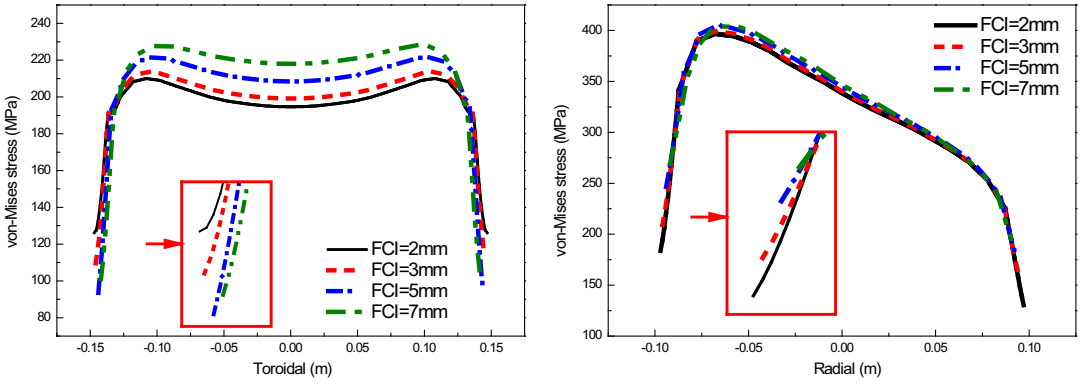

(a) von-Mises stresses on side wall (b) von-Mises stresses on Hartmann wall

Fig. 18. Von-Mises stresses at side wall and Hartmann wall of FCI with FCI thickness 2 mm, 3 mm, 5 mm and 7 mm.

overwhelm the toroidal one in the displacement vector sum distribution.

Fig. 18 indicates that stresses on side wall increase monotonously with the wall thickness increasing. However, for the stresses on Hartmann wall, the differences are much smaller. The 5 mm and 7 mm thick FCI can lead to slightly larger stresses than the 2 mm and 3 mm FCI. Moreover, since the thickness of FCI affects not only heat transfer but also fluid flow velocity, non-monotonic changes of stresses can be seen on the Hartmann wall when FCI thickness increases. The nonlinear coupling effect also results in the non-monotonic changes of

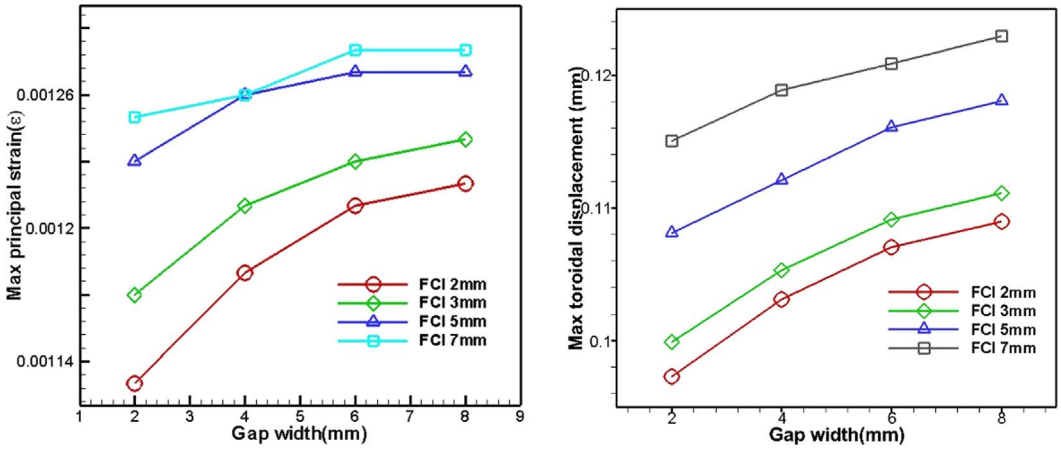

(a) The maximum principal strain (b) The maximum toroidal displacement

Fig. 19. The effects of geometrical configurations on strain and displacement of FCI.

displacement gradient and strain (see Fig. 19(a)), although the nonlinear effect has no evident influence on monotonic variation of toroidal displacement v.s. FCI thickness (see Fig. 19(b)).

6. Conclusions

Coupling magneto-thermo-fluid-structure fields are analyzed by using of CFD and FEM. A direct simulation of 3D liquid metal flow in the Dual Coolant Lead Lithium blanket is conducted to study the MHD effects and heat transfer influenced by geometry configuration of blanket. The basic effects on the velocity distribution, electric current streamlines and temperature distribution in blanket and thermal deformations of FCI structure are investigated. Summing up the results and analysis, the following conclusions are shown:

(1) Both thicker FCI and wider gap would increase the MHD pressure drops in bulk flow. The thickness of FCI has little influence on the pressure drop in gap flow. All 16 models can decrease pressure drop over 100 times compared to the cases without FCI.
(2) Although the thicker FCI has smaller displacement, its strain and stress would change monotonously because of the nonlinear coupling effect of fluid flow velocity and heat transfer.
(3) The wider gap would lead to higher jet velocity in side gap flow, which enhances the heat transfer performance. But wider gap may lead to larger stress in FCI.
(4) According to the effects caused by the FCI thickness and gap width, like MHD pressure drop, heat transfer efficiency and structure safety, we suggest the blanket structure with 5 mm FCI and 6 mm gap.

Although the increasing of FCI thickness or gap width can enhance the heat transfer, it could be harmful to structural safety. Thus, it is necessary to study coupling effect in magneto-thermo-fluid-structure field, which plays an important role in ITER design.

Acknowledgments

This work is performed with support from the National Natural Science Foundation of China, under grant no. 51376175, and the ITER project from the National Basic Research Program of China, under grant no. 2013GB114001.

References

[1] M.A. Abdou, Perspective on fusion energy, Proceedings of TWAS-ARO Meeting, Bibliotheca Alexandria, 2009, p. 4.
[2] M.S. Tillack, S. Malang, High Performance PbLi Blanket, Proceedings of the 17th IEEE/NPSS Symposium on Fusion Energy, San Diego, California, (1997), pp. 1000–1004.
[3] M.A. Abdou, D. Sze, C. Wong, M. Sawan, A. Ying, N.B. Morley, S. Malang, US plans and strategy for ITER blanket testing, Fusion Sci. Technol. 47 (2005) 475–487.
[4] N.B. Morley, Y. Katoh, S. Malang, B.A. Pint, A.R. Raffray, S. Sharaft, S. Smolentsev, G.E. Youngblood, Recent research and development for the dual coolant blanket concept in the US, Fusion Eng. Des. 83 (2008) 920–927.
[5] Z.Y. Xu, C.J. Pan, X.J. Zhang, L. Zhao, J. Zhang, G.J. Yang, Primary experimental results of MHD flow in the duct with flow channel insert, Nuclear Fusion and Plasma Physics, 29 2009, pp. 6–9.
[6] M.A. Abdou, N.B. Morley, A.Y. Ying, S. Smolentsev, P. Calderoni, Overview of fusion blanket R & D in the US over the last decade, Fusion Eng. Technol. 37 (2005) 401–422.
[7] D. Sutevski, S. Smolentsev, N.B. Morley, M.A. Abdou, 3D numerical study of MHD flow in a rectangular duct with flow channel insert, Fusion Sci. Technol. 50 (2006) 107–119.
[8] S. Smolentsev, M.A. Abdou, N.B. Morley, et al., Numerical analysis of MHD flow and heat transfer in a poloidal channel of the DCLL blanket with a SiCf/SiC flow channel insert, Fusion Eng. Des. 81 (2006) 549–553.
[9] S. Smolentsev, N.B. Morley, M.A. Abdou, Code development for analysis of MHD pressure drop reduction in a liquid metal blanket using insulation technique based on a fully developed flow model, Fusion Eng. Des. 73 (2005) 83–93.
[10] M.J. Ni, S.J. Xu, Z.H. Wang, N.M. Zhang, Direct simulation of three-dimensional MHD flows in liquid metal blanket with flow channel insert, Fusion Sci. Technol. 60 (2011) 292–297.
[11] S.J. Xu, M.J. Ni, Direct simulation of MHD flows in dual-coolant liquid metal fusion blanket using a consistent and conservative scheme, Theor. Appl. Mech. Lett. 1 (2011) 1–4.
[12] S. Smolentsev, N.B. Morley, M.A. Abdou, Magnetohydrodynamic and thermal issues of the SiCf/ SiC flow channel insert, Fusion Sci. Technol. 50 (2006) 107–119.
[13] S. Smolentsev, N.B. Morley, C. Wong, M.A. Abdou, MHD and heat transfer considerations for the US DCLL blanket for DEMO and ITER TBM, Fusion Eng. Des. 83 (2008) 1788–1791.
[14] D. Sutevski, S. Smolentsev, M.A. Abdou, 3D numerical study of pressure equalization in MHD flow in a rectangular duct with insulating flow channel insert, Fusion Sci. Technol. 89 (2014) 1370–1374.
[15] R.E. Alcouffe, R.S. Baker, F.W. Brinkley, DANTSYS 3.0: A Diffusion Accelerated Neutral Particle Transport Code System, LA-12969-M, Los Alamos National Laboratory, 1995.
[16] P.A. Davidson, An Introduction to Magnetohydrodynamics, first ed., Cambridge Texts in Applied Mathematics, (2001).
[17] C.P.C. Wong, M.A. Abdou, M. Dagher, Y. Katoh, R.J. Kurtz, S. Malang, E.P. Marriott, B.J. Merrill, K. Messadek, N.B. Morley, M.E. Sawan, S. Sharafat, S. Smolentsev, D.K. Sze, S. Willms, A. Ying, M.Z. Youssef, An overview of the US DCLL ITER-TBM program, Fusion Eng. Des. 85 (2010) 1129–1132.
[18] R. Issa, Solution of the implicitly discretized fluid flow equation by operator splitting, J. Comput. Phys. 62 (1986) 40–65.
[19] M.J. Ni, R. Munipalli, N.B. Morley, et al., A current density conservative scheme for incompressible MHD flows at a low magnetic Reynolds number. Part I: on a rectangular collocated grid system, J. Comput. Phys. 227 (2007) 174–204.
[20] M.J. Ni, R. Munipalli, P. Huang, et al., A current density conservative scheme for incompressible MHD flows at a low magnetic Reynolds number. Part II: on an arbitrary collocated mesh, J. Comput. Phys. 227 (2007) 205–228.
[21] M.J. Ni, J.F. Li, A consistent and conservative scheme for incompressible MHD flows at a low magnetic Reynolds number. Part III: on a staggered mesh, J. Comput. Phys. 231 (2012) 281–298.
[22] S. Vantieghem, X. Albets-Chico, B. Knaepen, The velocity profile of laminar MHD flows in circular conducting pipes, Theor. Comput. Fluid Dyn. 23 (2009) 525–533.
[23] J.C.R. Hunt, Magnetohydrodynamic flow in rectangular ducts, J. Fluid Mech. 21 (1965) 577–590.
[24] S. Timoshenko, J. Goodier, Theory of Elasticity, first ed., Cambridge university press, New York, 1951, p. 412.